Available online at www.sciencedirect.com
SCIENCE DIRECT®
ELSEVIER
Nuclear Instruments and Methods in Physics Research A 518 (2004) 764–774
NUCLEAR INSTRUMENTS & METHODS IN PHYSICS RESEARCH Section A
www.elsevier.com/locate/nima

GEANT4 code for simulation of a germanium gamma-ray detector and its application to efficiency calibration

S. Hurtado[a,*], M. García-León[a], R. García-Tenorio[b]

[a] Departamento de Física Atómica, Molecular y Nuclear, Facultad de Fisica, Universidad de Sevilla, Aptd. 1065, 41080 Sevilla, Spain
[b] Departamento de Física Aplicada II, Universidad de Sevilla, Spain

Received 31 July 2003; accepted 25 September 2003

Abstract

The GEANT4 software was developed by RD44, a world-wide collaboration of national institutes, laboratories and large High-Energy Physics experiments. GEANT4 is a public software package composed of tools which can be used to accurately simulate the passage of particles through matter. In this article, the first attempt to use GEANT4 to model a reverse electrode germanium detector (REGe), and to improve also its efficiency calibration procedure, is presented. A variance reduction algorithm based on a directional bias scheme is implemented into GEANT4 in order to accelerate the efficiency computations. A fast optimisation method to model the detector geometry using standard point sources is also presented and validated for point, Marinelli and air filter sources. The simulated full-energy peak efficiencies agreed with the measured values to within 1% between 36 and 1460 keV for these three counting geometries.

PACS: 29.30.Kv; 87.53.Wz

Keywords: Gamma-spectrometry; Efficiency calibration; Efficiency transfer; Monte Carlo simulation; Optimised detector model; GEANT4; Variance reduction

1. Introduction

The Monte Carlo code GEANT3 was first developed in FORTRAN at CERN to simulate the passage of particles through matter [1]. The new GEANT4 project [2] came up in 1994 to improve the existing GEANT3 program. The design choice of GEANT4 was an object-oriented methodology and C++ language in order to provide modular and flexible software. The comparison of the simulation results using GEANT3 and GEANT4 electro-magnetic physics processes demonstrates that, in general, they are very close [3]. However, in some cases GEANT4 is more adequate and its physics is extended beyond GEANT3. In GEANT3 the secondary radiations (X-rays and Auger electrons) following photo-electric effect are not considered. Moreover, another limitation of GEANT3 is that it does not simulate a particle when its energy is less than 10 keV. This means, for instance, that Ge X-rays escape cannot be processed and this is very important for a rigorous γ-spectrometry simulation. GEANT4 can overcome all this difficulties

*Corresponding author. Tel.: +34-954550928; fax: +34-954554445.
E-mail address: shurtado@us.es (S. Hurtado).

0168-9002/$ - see front matter © 2003 Elsevier B.V. All rights reserved.
doi:10.1016/j.nima.2003.09.057

since it includes low-energy electro-magnetic processes [4] down to 250 eV. For these reasons, we decided to develop a simulation package of the low-level gamma-ray spectrometer REGe presented in our laboratory using GEANT4 for the first time.

GEANT4 is a toolkit which the user must implement by himself. Indeed, to build a simulation package the user must implement several classes to describe the detector geometry (materials used, detector sensitive components, etc.), the primary particle generator (particle type, and energy, position and direction distributions), the relevant particles and physics processes. A firm knowledge of object-oriented programming is required to implement all these user classes and to overload standard GEANT4 functionality.

In order to check the application of the GEANT4 simulation package to low-level gamma-ray spectrometry, we have calculated the precise full-energy peak (f.e.p.) efficiency calibration of our detector. Experimental efficiency calibration is a difficult and time-consuming procedure for each specific geometry. To overcome such problem, different non-experimental methods are currently used, such as semi-empirical computation [5–8] or Monte Carlo simulation [9–14]. Semi-empirical methods are based mostly on the principle described by Moens et al. [15]. These semi-empirical methods are simple and fast, but usually not accessible for public use. They are also restricted to limited source–detector geometries because they involve some approximations and simplifications in their calculations [15,16].

Analog Monte Carlo methods are based in determining f.e.p. efficiency by simulating all relevant physical processes taking place along the path of a photon emitted by the source. The history of each individual primary particle consists of its emission by the source, interaction with the detector and surrounding materials, production as well as transport of secondary particles, and track until the photon escapes or undergoes a photoelectric interaction in the crystal, depositing all of its energy. Since no approximations are needed, there is no limitation on the source–detector configuration. The main disadvantage of these analog Monte Carlo calculations is that a large number of histories ($> 10^5$–10^6 primary photons) must be simulated to obtain a statistical uncertainty of less than 1%. Therefore, analog Monte Carlo methods need long computing times. It is thus desirable to introduce a variance reduction technique to improve its computational efficiency (non-analog Monte Carlo method) [5]. In this paper we introduce a simple variance reduction scheme based on directional bias. The goal of this method is to simulate only primary photons that are emitted from the sample in directions towards the detector active volume.

Moreover, all Monte Carlo codes generally give computed values that deviate significantly (> 10%) from the experimental efficiency data, due to uncertainties associated to the values of the detector parameters supplied by manufacturer and/or incomplete charge collection in the crystal. The incomplete charge collection can be overcome solving the Poisson differential equation for the potential and the electric field inside the detector crystal [17]. But this procedure does not completely match the experimental and simulated values of the efficiency. Therefore we have to optimise some detector parameters (i.e. crystal-to-window distance and dead-layer thickness) since these are usually not sufficiently accurate in the manufacturer's specification [9,11,12,18]. In this paper a well determined procedure is developed to obtain a suitable set of optimised parameters in order to calculate the f.e.p. efficiency of a Ge detector for point, Marinelli beaker and air filter geometries.

2. Experimental data

2.1. Experimental arrangement

Measurements were performed with a Canberra n-type Reverse electrode Germanium (ReGe) detector, with a relative photo-peak efficiency of 30% at 1332 keV. The nominal dimensions supplied by the manufacturer are in Table 1. A radiography of the detector was taken and we check that there was not any displacement of the crystal from the axis of the housing. A lead shield (10 cm thick regular lead) and an inner copper layer (5 mm) surround the detector to protect it

Table 1
Detector dimensions as specified by the manufacturer and as optimised by Monte Carlo simulations

Detector parameter	Nominal (mm)	Optimised (mm)
Ge crystal-to-Be window distance (D)	5	7.4
Ge crystal radius (R)	27	27
Ge crystal length (L)	55	55
Ge front dead layer (t_f)	3×10^{-4}	3×10^{-2}
Hole radius (r)	0.5	0.65
Hole inner dead layer (t_h)	0.5	1.0
Hole length (l)	41	41
Be window thickness (w)	0.5	0.5

against environmental radiation. The preamplified signals from the detector are sent to a Canberra Spectroscopy Amplifier model 2020 and an Canberra ADC model 8701 connected to an *Accuspec*™ card. Gamma-ray peaks are analysed with *Genie2K*™ using a gaussian peak with a step background fit.

2.2. Experimental efficiency calibration

The detector was calibrated using standard point and solution sources. These sources include four isolated emission radionuclides (^{210}Pb, ^{241}Am, ^{137}Cs and ^{40}K) and two cascade emission radionuclides (^{133}Ba and ^{152}Eu).

The efficiency ε for a given photon energy is obtained from:

$$\varepsilon = \frac{N}{TAp} C_i \quad (1)$$

where N is the number of net counts in the peak, T is the measuring time, A is the radionuclide activity, p is the photon emission probability [19] and C_i are corrections factors due to dead time, radionuclide decay and coincidence-summing corrections. The dead time never exceeded 1%, so the corresponding correction factor was obtained simply using ADC live time. The radionuclide decay was also taken into account. The statistical uncertainties of the net peak areas were smaller than 0.5%, since the acquisition time was long enough and background subtraction was negligible. Such values were below or close to the corresponding uncertainties of the photon emission probabilities. The main source of uncertainty in the relative efficiency calculation was the uncertainties in the activities of the standard solutions (see Section 2.3). Coincidence-summing effects are negligible in the reference measuring geometry [20] described below, and they are also not present for the isolated emissions of the standard sources used in the other measuring geometries.

Once the efficiencies have been fixed by applying the correction factors, the overall efficiency curve is obtained by fitting the experimental points to a polynomial logarithmic function of fourth order using a non-linear least-squares fit. The non-linear least-squares analysis has been performed by Levenberg–Marquardt method using the covariance matrix of the experimental data [21]. In that manner, the correlation between data points from the same calibrated source has been included to avoid the overestimation of experimental efficiency uncertainties.

2.3. Point sources

Calibration sources were obtained using standard solutions that contain: ^{210}Pb (105.8 ± 0.4 Bq/g) and ^{241}Am (329 ± 1 Bq/g) supplied by CIEMAT (Madrid, Spain); and ^{137}Cs (53.7 ± 0.8 kBq/g), ^{133}Ba (29.74 ± 0.44 kBq/g) and ^{152}Eu (54.6 ± 1.1 kBq/g) supplied by DAMRI (France). Point calibration sources (P) were obtained by pipetting and drying a volume of standard solutions over aluminium planchets. The ^{40}K source were obtained by packing 10 g. of KCl from Merck.

The reference geometry was a point-like source measured at 15.9 cm source-to-detector window distance to avoid coincidence-summing effect. In order to adjust the detector parameters, the efficiency is also experimentally determined with the isolated emission point sources at 3.6 cm in front of the detector window, and at a distance of 8.2 cm from the side of the detector. The experimental efficiency points for reference geometry are shown in Table 2. The corresponding reduced chi-square value is 0.5 for a polynomial fit, and

Table 2
Calculated efficiencies and relative deviation RD(%) between the experimental and computed efficiencies for the point geometry at the reference position

Energy (keV)	ε_{exp}	ε_{MC}	RD(%)	ε_{MC}^{opt}	RD(%)
36.3	0.570(20)	0.671(4)	17.2	0.572(3)	0.07
46	0.617(11)	0.650(3)	5.34	0.614(3)	−0.45
59	0.632(8)	0.651(3)	2.88	0.635(3)	0.34
81	0.637(14)	0.637(3)	−0.04	0.632(3)	−0.87
121	0.583(11)	0.588(3)	0.83	0.585(3)	0.19
276	0.339(8)	0.349(3)	2.90	0.335(4)	−1.57
356	0.264(5)	0.275(4)	4.17	0.264(4)	−0.71
661	0.146(2)	0.157(4)	7.32	0.146(4)	−0.40
778	0.126(3)	0.138(5)	9.04	0.127(5)	0.19
964	0.104(3)	0.115(6)	10.64	0.106(6)	1.4
1112	0.094(3)	0.103(7)	9.41	0.095(7)	1.2
1460	0.077(2)	0.0821(7)	7.56	0.0756(7)	−0.80
Mean			6.45		0.68
RMS			0.40		0.04

ε_{exp} indicates the experimental values, ε_{MC} refers to the calculated efficiencies with nominal parameters, and ε_{MC}^{opt} is for optimised geometry method. Mean and RMS error of the absolutes values of the deviations for the whole energy range are shown in the last two rows.

Table 3
Calculated efficiencies and relative deviation RD(%) between the experimental and computed efficiencies for Marinelli beaker and air filter

Energy (keV)	ε_{exp}	ε_{MC}	RD(%)	ε_{MC}^{opt}	RD(%)
Marinelli beaker					
36.3	2.22(10)	2.835(7)	27.3	2.217(6)	−0.47
46.56	3.077(53)	3.396(8)	10.4	3.106(6)	0.93
59.53	3.635(55)	3.837(8)	5.5	3.630(6)	−0.15
661.6	1.081(9)	1.117(6)	3.44	1.069(6)	−1.08
1460.8	0.560(8)	0.608(3)	8.5	0.565(3)	0.81
Mean			11.0		0.69
RMS			0.79		0.03
Air filter					
36.3	4.11(17)	5.004(7)	21.6	4.050(5)	−1.5
46.56	4.76(6)	5.683(8)	19.4	4.800(6)	0.88
59.53	5.22(9)	5.899(8)	13.0	5.233(6)	0.27
661.6	1.206(18)	1.359(6)	12.7	1.206(6)	−0.02
1460.8	0.608(81)	0.708(3)	16.2	0.609(3)	0.13
Mean			16.6		0.56
RMS			0.33		0.05

ε_{exp} indicates the experimental values, ε_{MC} refers to the calculated efficiencies with nominal parameters, and ε_{MC}^{opt} is for optimised geometry method. Mean and RMS error of the absolutes values of the deviations for the whole energy range are shown in the last two rows.

the resulting uncertainties are around 0.94% at 60 keV, 0.56% from 100 to 500 keV, and 0.28% between 500 and 1500 keV.

2.4. Volume sources

The experimental detector efficiency was also determined for 1 litre Marinelli beaker containing water (M), and for polyethylene air filter (F) geometries. The Marinelli beaker source was placed at a distance of 0.9 cm above the detector window. The Marinelli beaker's dimensions were 12.5 cm diameter and 15.4 cm height, the dimensions of its inner holder being 7.9 cm diameter and 7.6 cm ring height. The polyethylene filter was folded four times to make a rectangular parallelepiped of approximate size $5.9 \times 5.9 \times 0.6$ cm^3, and it was located at 1.1 cm above the detector window. Both geometries set-ups were homogeneously spiked using the previous isolated emission standard solutions supplied by CIEMAT and DAMRI (^{210}Pb, ^{241}Am, ^{137}Cs and ^{40}K), which activity was determined by gravimetry. The resulting experimental points are shown in Table 3.

3. Monte Carlo simulation

In GEANT4, the following electro-magnetic processes needed for gamma-ray spectrometry are included: Compton scattering, photo-electric effect, Rayleigh effect, pair production, multiple scattering, fluorescence and Auger effect, bremsstrahlung and ionisation. In GEANT4 a new code of electro-magnetic interaction for low energy has been developed [4] and valid energy range is extended to 250 eV. This enhancement is based on the use of experimental data parameterisations using the following databases developed by the Lawrence Livermore National Laboratory: EPDL97 (Evaluated Photon Data Library),

EEDL (Evaluated Electron Data Library) and EADL (Evaluated Atomic Data Library). This low threshold, together with the physics processes available, allows us to use GEANT4 for simulating the energy response of our ReGe detector.

3.1. Model of the detector

The detector set-up was firstly modelled using the technical dimensions supplied by the manufacturer (see Fig. 2). The detector structure can be easily described to the simulation program using a variety of geometrical elements available in GEANT4. A series of cones and discs were used in order to describe the germanium crystal, inactive hole, beryllium window, endcap, holder and dead layers. According to the information from the manufacturer, the detector crystal has rounded edges. Therefore, the dimensions describing the rounding off of the crystal edges were adjusted using the information obtained from the radiography taken. The external dead layer consists of a ion(boron)-implanted p+ contact. The inner n+ contact is made of a germanium layer which lithium atoms diffused in. The manufacture procedure to obtain the dimensions of these dead layers is not know, so we consider them only an estimation.

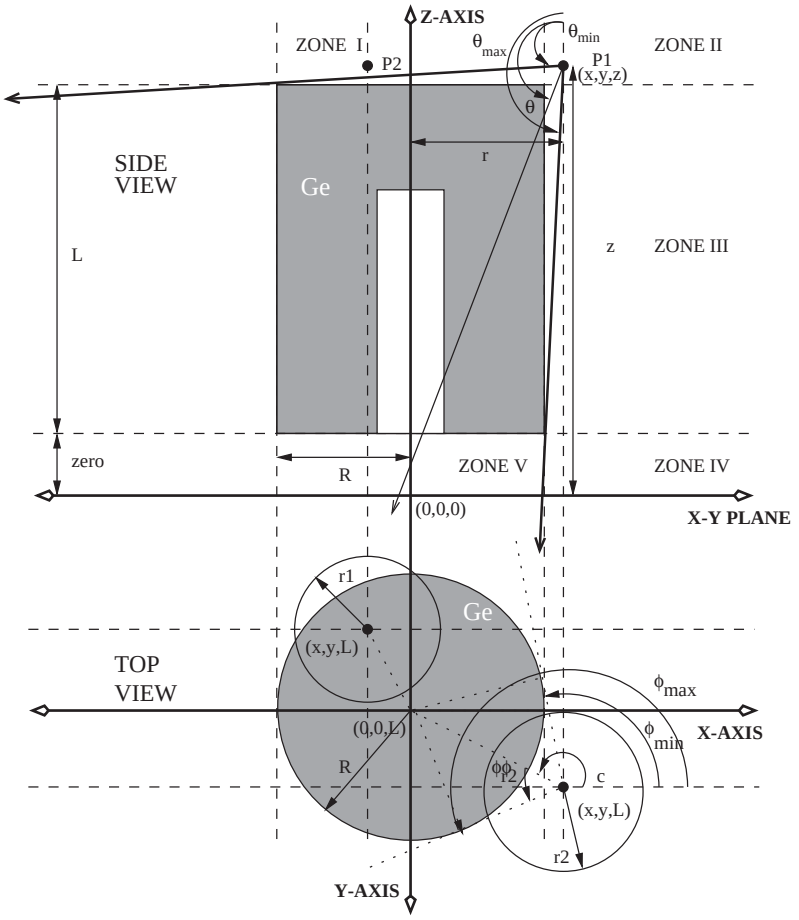

Fig. 1. Principal trigonometric parameters in variance reduction algorithm. The space surrounding the Ge crystal is divided into five zones. Depending where the emission point is (i.e. P1 in zone II or P2 in zone I), the trigonometric equations change in order to obtain the correct values of θ_{min}, θ_{max}, ϕ_{max} and ϕ_{min}. The rest of trigonometric parameters are explained in Section 3.2.

3.2. Variance reduction method

An analog Monte Carlo (MC) simulation may require an unacceptable long time to produce statistically relevant results. It is thus desirable to reduce the computing time by introducing a variance reduction technique: directional bias method. The source photon emission is isotropic in analog MC simulations. Therefore the solid angle of the detector acceptance is small due to the size of the detector crystal itself. Only a few percent of the photons generated and tracked in analog MC simulations will actually be directly detected, so the non-analog MC simulation only generates photons that are emitted in the direction towards the detector crystal. We have to point out that this technique is only valid for f.e.p. efficiency calculations. For this purpose, we have implemented in GEANT4 a simplified algorithm based in Ref. [5] to be used in our simulation. But we have encountered some problems applying to our geometry set-up the original equations present in that work. In fact at some points surrounding the detector crystal, the efficiency calculated using an isotropic flux does not match the efficiency calculated using the original directional bias equations. Thus, we have modified the original trigonometric equations to obtain a correct efficiency calculation. Besides we have also implemented new trigonometric equations in order to extend the possible region of emission below the detector crystal. This will be useful for simulate measurement geometries like Marinelli beaker.

The trigonometric relations are shown in Fig. 1 where the geometry set-up is divided into five zones. The detector crystal, with radius R and height L, is situated at a distance $z = \text{zero}$. For this geometry set-up a sampling of the azimuthal angle ϕ and the polar angle θ was calculated from the maximum and minimum acceptance angles $(\phi_{\min}, \phi_{\max})$ and $(\theta_{\min}, \theta_{\max})$:

$$\theta = \cos^{-1}[\cos\theta_{\min} - n_1(\cos\theta_{\min} - \cos\theta_{\max})] \quad (2)$$

$$\phi = n_2(\phi_{\max} - \phi_{\min}) + \phi_{\min} \quad (3)$$

with n_1 and n_2 random numbers. The acceptance angles for a photon, generated in the position (x, y, z) within the source, are obtained with the next expressions:

$$\theta_{\min} = \begin{cases} \tan^{-1}\left[\dfrac{r-R}{L-(z-\text{zero})}\right] & \text{if } r \geqslant R \text{ and } z < (L+\text{zero}) \text{ [zones III, IV]} \\ \pi - \tan^{-1}\left[\dfrac{r+R}{(z-\text{zero})-L}\right] & \text{if } z \geqslant (L+\text{zero}) \text{ [zones I, II]} \\ 0 & \text{if } r < R \text{ and } z < \text{zero [zone V]} \end{cases} \quad (4)$$

$$\theta_{\max} = \begin{cases} \pi & \text{if } r < R \text{ and } z \geqslant (L+\text{zero}) \text{ [zone I]} \\ \tan^{-1}\left[\dfrac{r+R}{|z-\text{zero}|}\right] & \text{if } r < R \text{ and } z < \text{zero [zone V]} \\ \pi - \tan^{-1}\left[\dfrac{r-R}{|z-\text{zero}|}\right] & \text{if } r \geqslant R \text{ and } (z-\text{zero}) \geqslant 0 \text{ [zones II, III]} \\ \tan^{-1}\left[\dfrac{r+R}{|z-\text{zero}|}\right] & \text{if } r \geqslant R \text{ and } (z-\text{zero}) < 0 \text{ [zone IV]} \end{cases} \quad (5)$$

$$\phi_{\min} = \begin{cases} 0 & \text{if } r < R \text{ and } (r+r_1) \leqslant R \text{ and } z > (L+\text{zero}) \text{ [zone I]} \\ 0 & \text{if } r < R \text{ and } (r+r_2) \leqslant R \text{ and } z < \text{zero [zone V]} \\ \phi_c - \phi_{r1} & \text{if } r < R \text{ and } (r+r_1) > R \text{ and } z > (L+\text{zero}) \text{ [zone I]} \\ \phi_c - \phi_{r3} & \text{if } r < R \text{ and } (r+r_2) > R \text{ and } z < \text{zero [zone V]} \\ \phi_c - \phi_{r2} & \text{if } r \geqslant R \text{ [zone II, III, IV]} \end{cases} \quad (6)$$

$$\phi_{\max} = \begin{cases} 2\pi & \text{if } r<R \text{ and } (r+r_1)\leqslant R \\ & \text{and } z>(L+\text{zero}) \text{ [zone I]} \\ 2\pi & \text{if } r<R \text{ and } (r+r_2)\leqslant R \\ & \text{and } z<\text{zero [zone V]} \\ \phi_c+\phi_{r1} & \text{if } r<R \text{ and } (r+r_1)>R \\ & \text{and } z>(L+\text{zero}) \text{ [zone I]} \\ \phi_c+\phi_{r3} & \text{if } r<R \text{ and } (r+r_2)>R \\ & \text{and } z<\text{zero [zone V]} \\ \phi_c+\phi_{r2} & \text{if } r\geqslant R \text{ [zone II, III, IV]} \end{cases} \tag{7}$$

where

$$\phi_c = \begin{cases} 2\pi+\tan^{-1}(y/x) & \text{if } x<0, \\ \pi+\tan^{-1}(y/x) & \text{if } x\geqslant 0. \end{cases} \tag{8}$$

$$r_1 = |(z-\text{zero}-L)\tan\theta| \tag{9}$$

$$r_2 = |(z-\text{zero})\tan\theta| \tag{10}$$

$$\phi_{r1} = \cos^{-1}[r^2+r_1^2-R^2/2r_1r] \tag{11}$$

$$\phi_{r2} = \sin^{-1}[R/r] \tag{12}$$

$$\phi_{r3} = \cos^{-1}[r^2+r_2^2-R^2/2r_2r]. \tag{13}$$

The parameters r_1 and r_2 represent, respectively, the radius of the intersection between the θ-cone and the upper and lower plane of the detector crystal. The angles ϕ_c, ϕ_{r1}, ϕ_{r2} and ϕ_{r3} are used to calculate the position of the source point referring to the detector centre axis in cartesian coordinates. For a source point located at height z and radius r (i.e. P1 in zone II and P2 in zone I), the above expressions [2–7] give us the ranges $(\phi_{\min},\phi_{\max})$ and $(\theta_{\min},\theta_{\max})$.

Since we have forced the photon to interact within the acceptance angles we must weight the quantities scored resulting from this interaction. The weighting factor takes the form:

$$w = (\cos(\theta_{\min})-\cos(\theta_{\max}))(\phi_{\max}-\phi_{\min})/4\pi. \tag{14}$$

Also, we require a reliable figure of merit (FOM) to estimate the improvement of the variance reduction technique in comparison with the isotropic flux. The FOM is given by the expression $\text{FOM} = 1/\sigma^2 T$, where T is the computing time used (CPU hours) and σ is the variance associated to the calculated result as can be seen in Section 3.3. In order to compare correctly the FOM values for variance reduction technique and the isotropic flux, the variance obtained is always around 0.5% in both types of simulation. We obtained a FOM value for each geometry using an isotropic flux: $(\text{FOM})_{\text{P}}^{\text{iso}} = 0.13$, $(\text{FOM})_{\text{M}}^{\text{iso}} = 0.08$ and $(\text{FOM})_{\text{F}}^{\text{iso}} = 0.12$, for point, Marinelli, and air filter geometries, respectively. If we use the variance reduction method the obtained FOM values are: $(\text{FOM})_{\text{P}}^{\text{bias}} = 0.50$ $(\text{FOM})_{\text{M}}^{\text{bias}} = 0.36$ and $(\text{FOM})_{\text{F}}^{\text{bias}} = 0.47$. The higher values for the FOM reflects that the variance reduction technique can improve the Monte Carlo simulation doing it four times faster without affecting the variance of the computed results.

3.3. Monte Carlo data analysis

In the Monte Carlo simulation the relevant physical quantity is the energy deposited into the detector crystal. The results obtained by non-analog simulation are biased by the variance reduction technique and a correction for this is required. A particle history weight w is introduced (see Eq. (14)) and calculated for each particle history. If an event occurs, the weight w is added to the corresponding energy in the histogram rather than incrementing by one unit. In this way the weight is implicitly included into the peak area and so the expectation value of the f.e.p. efficiency is preserved. In order to compare calculated and experimental efficiencies it is necessary to simulate the statistical fluctuations in the process of charge carrier production and pulse electronic analysis. For this purpose, a gaussian distribution with parameters (mean $\bar{x}$ and standard deviation σ) extracted from experimental data is applied to the deposited energy E_0 [10]. Firstly, we compute the experimental resolution (FWHM) at the deposited energy FWHM(E_0). The next step consists of generate a random energy (E_{r}) using a gaussian distribution with $\bar{x} = E_0$ and $\sigma = 2.355\times$ FWHM(E_0). If the random energy is in the interval $E_0 \pm 2.96\sigma$, it belongs to the peak at energy E_0. Then the gaussian distributed spectrum is processed by an algorithm written in C++ into the ROOT [22] analysis framework. It performs a

peak search process, and an area and step background calculation using the same mathematical algorithm like in *Genie*2K^{TM}. The weighted peak area divided by the full number of photons emitted of the energy of interest gives the f.e.p. efficiency. In order to estimate the uncertainties associated to the calculated efficiency, we make ten independent runs ($m = 10$) of the Monte Carlo simulation for each energy of emission. Thus, the final calculated efficiency (ε) is given by the mean of the calculated efficiencies (ε_k) for each simulation run at a particular energy:

$$\varepsilon = \frac{1}{m}\sum_{k=1}^{m}\varepsilon_k \tag{15}$$

and an estimation of the variance of the efficiency (σ) is given by the expression [20]:

$$\sigma_\varepsilon^2 = \frac{1}{m-1}\sum_{k=1}^{m}(\varepsilon_k - \varepsilon)^2. \tag{16}$$

3.4. Monte Carlo simulation

The main disadvantage of the efficiency calculation by using Monte Carlo method is the not sufficient reliability in detector parameters provided by the manufacturer. The efficiency values computed with the supplied detector data (Table 1) deviate significantly (around 10%) from the experimental data for all the measuring geometries. In order to reject a problem of the physics models a comparative simulation was carried out using GEANT4 standard electro-magnetic physics and GEANT4 low energy electro-magnetic physics. The results obtained were in good agreement except, of course, at low energies. On the other hand, the radiography of the detector reflected a possible value (0.65–0.85 cm) of the crystal to window distance bigger than the nominal value given by the manufacturer (0.5 cm). Therefore the detector parameters have to be optimised in order to obtain better agreement among computed and experimental data. The detector model constructed in that way can be used to compute the efficiencies for a new geometry set-up.

In Fig. 2 is shown a plan drawing of the REGe detector with the most critical parameters that affect the efficiency calculation. According to the manufacturer, the detector radius (R) and length (L) are known with sufficient confidence in modern detectors ($R = 27 \pm 1$ mm, $L = 55 \pm 1$ mm).

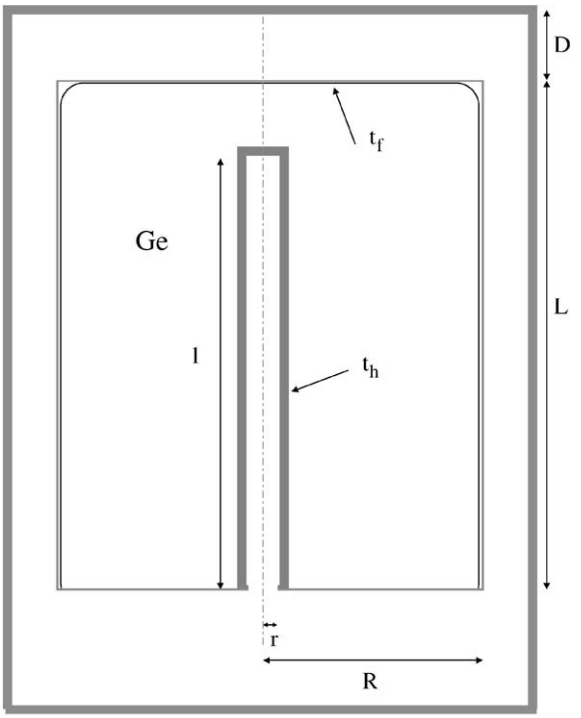

Fig. 2. Detector geometry. Dimensions given in Table 1 are identified by the same letters in the figure.

The main strategy consists of a comparison between experimental and calculated f.e.p. efficiency for different detector parameter set-ups at the reference geometry. Firstly, the detector radius is modified (R_{mod}), and then, the optimum crystal-to-window distance (D_{opt}) is calculated. Using this optimum value the front dead layer thickness (t_f^{opt}) is varied until the best efficiency values are obtained at the 36–81 keV range. Finally, the detector length L and the parameters of the inner inactive hole (t_h, h and r) are also checked.

The first step consists of determining the thickness of the front dead-layer (t_f) and the crystal-to-Be window distance (D), and also checking R. To determine these parameters we obtained the experimental efficiencies for the

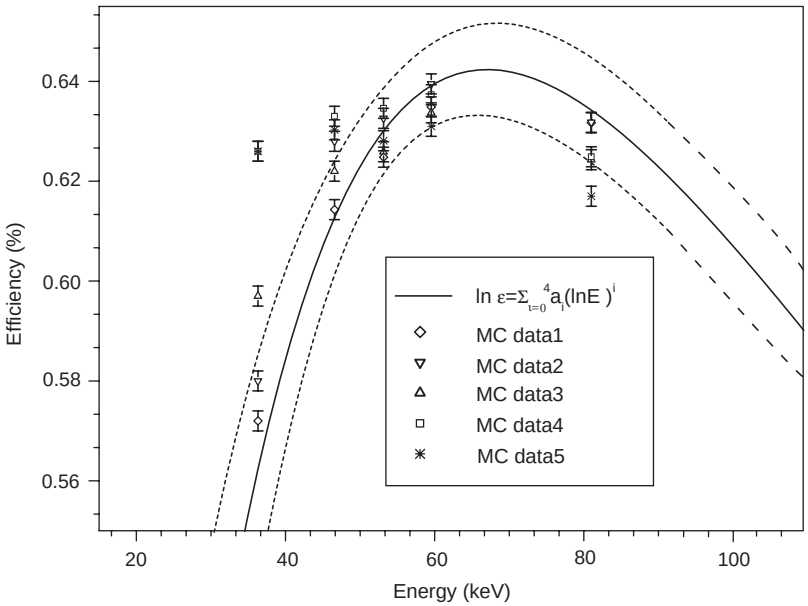

Fig. 3. Comparison of experimental (solid line) and calculated f.e.p. efficiency for different detector parameter set-ups at the reference geometry. The 95% prediction bands are shown as dashed lines. The detector radius (R_{mod}) is modified, and then, the optimum crystal-to-window distance (D_{opt}) is calculated. The front dead layer thickness (t_f^{opt}) is varied until the best efficiency values are obtained at the 37–81 keV range. The parameter values for each Monte Carlo data sets are: MC data set 1 ($R_{mod} = R$, $D_{opt} = D + 2.4$ mm, $t_f^{opt} = t_f + 29.7$ μm), MC data set 2 ($R_{mod} = R - 0.15$ mm, $D_{opt} = D + 2.4$ mm, $t_f^{opt} = t_f + 22.2$ μm), MC data set 3 ($R_{mod} = R - 0.25$ mm, $D_{opt} = D + 2.5$ mm, $t_f^{opt} = t_f + 14.5$ μm), MC data set 4 ($R_{mod} = R - 0.35$ mm, $D_{opt} = D + 2.5$ mm, $t_f^{opt} = t_f + 2.9$ μm) and MC data set 5 ($R_{mod} = R - 0.5$ mm, $D_{opt} = D + 2.7$ mm, $t_f^{opt} = t_f$); being R, D and t_f the nominal values of the detector parameters.

59.53 keV gamma-ray from ^{241}Am (see Section 2.3) at two distances (15.9 and 3.6 cm) from the beryllium window. Then we compute the efficiencies at these two distances while varying D for different values of the modified detector radius (R_{mod}), and remaining t_f fixed at its nominal value. After comparing the ratio of computed efficiencies at two distances with the experimental one, an optimised value for D is obtained (D_{opt}) for each value of R_{mod}. In order to select the correct value of R, we measured the experimental efficiencies at 36.3 keV (X-ray from ^{137}Cs), 46.53 keV (^{210}Pb), 53.15 keV (^{133}Ba), 59.53 keV (^{241}Am) and 81 keV (^{133}Ba) for a distance of 15.9 cm from the beryllium window. Because the values of t_f affects only gamma-rays below a few hundred keV, we compute the efficiencies at these five energies, for each value of R and D_{opt}, to reach an exact agreement while varying the thickness t_f. Good agreement required the detector radius to be fixed at the nominal value, and the dead-layer to be 29.7 μm thick as shown in Fig. 3. As can be seen in this figure the MC data 1 are the only values that totally lie within the 95% prediction band. The final values of these optimised parameters can be shown at Table 1.

In order to check L dimension, we calculate the efficiency of ^{137}Cs and ^{241}Am sources at 8.2 cm from the side of the detector obtaining a good agreement with its nominal value. Therefore, we keep the detector length L fixed at the nominal value provided by the manufacturer.

The three remaining parameters are the inner dead-layer (t_h) and the hole radius (r) that affect to high-energy gamma-rays above a few hundred keV. The hole radius was selected as free parameter, and not hole depth (l) that remains fixed, because according to Lèpy [18] this parameter affects the efficiency much more than the hole depth. We use the 1460.8 keV gamma-ray

from ^{40}K and the 661.6 keV gamma-ray from ^{137}Cs at a 15.9 cm distance for point source geometry. We compute the efficiencies for the two last energies while varying the values of r and t_h. The optimum values of the parameters were selected to obtain the best agreement between experimental and calculated efficiencies at these two high energies. The final detector dimensions are shown in Table 1.

4. Results

The results for point geometry set-up are given in Table 2 as the relative deviation (%) between the computed and experimental efficiency $100 \times (\varepsilon_{MC} - \varepsilon_{exp})/\varepsilon_{exp}$ for Monte Carlo method using nominal and optimised detector parameters. The mean and root mean square error (RMS) of relative deviation are presented to estimate the accuracy of each case. It can be noted that the results obtained with the nominal detector parameters show significant deviations. The mean discrepancy of 5% between the calculated and experimental f.e.p. efficiency can be due to an inadequate knowledge of the detector geometry and to imperfect charge collection in detector crystal. As commented before, in the present work various detector parameters have been changed in order to reduce the discrepancies between the experimental and calculated efficiencies (see Table 1). The optimum value of t_f is not implausible because nominal dead layers depth are only estimates, and imperfect charge collection can affect the experimental efficiency at these energies. It can be pointed out also that the final value of t_h can be higher than the nominal value due to the detector was warmed up after manufacture it. The other modified parameter was the crystal-to-window distance D. This parameter depends of the assembly and can be several millimetres higher than the nominal value provided by the manufacturer. In all the simulations we have taken into account the bulletized edge of the crystal. This characteristic was modelled using conical shapes available in GEANT4.

Once the detector geometry has been adjusted, the efficiency for other measurement geometries was computed using the optimum parameter values. The obtained calculated efficiencies are shown in Table 3 for the isolated emission energies (^{210}Pb, ^{241}Am, ^{137}Cs and ^{40}K). We can see that the agreement between the experimental and calculated efficiencies is good at low and high-energy range for Marinelli beaker and air filter. The mean absolute values of the deviations between the experimental and computed efficiencies using the optimised parameters for the whole energy range is reduced to 0.6% for these volume sources (see Table 3). When using nominal detector parameters the average of such deviations is around 10%. The improvement is clearly apparent. Therefore, we can conclude that the geometry optimisation process is correct and can be applied to the measurement of the specific activity of samples with irregular shapes.

5. Conclusions

With the GEANT4 Monte Carlo code, we have simulated the response of a low-level REGe germanium detector. A set of new classes have been developed into GEANT4. The analysis of the simulation data was performed implementing mathematical algorithms in a new C++ class. Moreover, a variance reduction algorithm has been validated and implemented into GEANT4 toolkit for f.e.p. efficiency calculation. Using this algorithm the simulations are four times faster than an isotropic one for different measurement geometries. This algorithm can be applied to real-time measurement conditions like in situ spectrometry.

In addition, we have simulated with the GEANT4 Monte Carlo code the efficiency response of the REGe detector. In our simulations we used first the nominal dimensions provided by the manufacturer that do not reflect the efficiencies at whole energy range. For that reason a fast procedure for geometry optimisation have been carried out with calibrated point sources. The optimised detector parameters remain realistic. A good agreement is reached between experimental and computed efficiencies using the optimised geometry for the three counting geometries.

Therefore the Monte Carlo method allows us to calculate the efficiency calibration curve for any source geometry that can be present in low-level background measurements.

Acknowledgements

This work has been partially supported by the Spanish Education Project BFM2001-3880, the EU project FIGECT-2000-00108 (ADVANCE) and the EU project FIGE-CT2000-00085 (REMOTRANS).

References

[1] Geant3 Home Page, http://wwwinfo.cern.ch/asd/geant/
[2] Geant4 Home Page, http://www.cern.ch/geant4
[3] S. Agostinelli, et al., Nucl. Instr. and Meth. A 506 (2003) 250.
[4] S. Giani, et al., CERN-OPEN-99-121, INFN-AE-99-20, INFN-AE-99-21, CERN-OPEN-99-300, Technical Report, CERN, 1999.
[5] S. Jiang, et al., Nucl. Instr. and Meth. A 413 (1998) 281.
[6] O. Sima, D. Arnold, Appl. Radiat. Isot. 56 (2002) 71.
[7] T. Wang, et al., Appl. Radiat. Isot. 46 (1995) 933.
[8] H. Aaltonen, S.K. Nad, F. Ugletveit, Nucl. Instr. and Meth. A 339 (1994) 87.
[9] J.C. Hardy, et al., Appl. Radiat. Isot. 56 (2002) 65.
[10] J.-M.Laborie, G.L. Petit, D. Abt, M. Girard, Appl. Radiat. Isot. 53 (2000) 57.
[11] T. Vidmar, A. Likar, Appl. Radiat. Isot. 56 (2002) 99.
[12] M. García-Talavera, H. Neder, M.J. Daza, B. Quintana, Appl. Radiat. Isot. 52 (2000) 777.
[13] M. Korun, A. Likar, T. Vidmar, Nucl. Instr. and Meth. A 390 (1997) 203.
[14] B. Braizinha, J. Ribeiro, A. Jesus, L. Peralta, Efficiency calibration of gamma-ray detectors by Monte-Carlo methods, in: Proceedings of the VIII International Conference on Calorimetry in High Energy Physics, World Scientific, Singapore, 2000.
[15] L. Moens, et al., Nucl. Instr. and Meth. 187 (1981) 451.
[16] D. Karamanis, V. Lacoste, S. Andriamonje, G. Barreau, M. Petit, Nucl. Instr. and Meth. A 487 (2002) 477.
[17] F. Hernández, F. El-Daoushy, Nucl. Instr. and Meth. A 498 (1–3) (2003) 340.
[18] M. Lépy, et al., Appl. Radiat. Isot. 55 (2001) 493.
[19] R.B. Firestone, Table of Isotopes, 8th Edition, Wiley, New York, 1996.
[20] K. Debertin, R.G. Helmer, Gamma and X-ray Spectrometry with Semiconductors Detectors, North-Holland, Amsterdam, 1988.
[21] L.P. Geraldo, D.L. Smith, Nucl. Instr. and Meth. A 290 (1990) 499.
[22] R. Brun, F. Rademakers, Nucl. Instr. and Meth. A 389 (1997) 81.